Thermodynamic Analysis of Cavity Creating Mutations in an Engineered Leucine Zipper and Energetics of Glycerol-Induced Coiled Coil Stabilization†

Eberhard Dürr‡ and Ilian Jelesarov*

Biochemisches Institut der Universität Zürich, Winterthurerstrasse 190, CH-8057 Zürich, Switzerland

Received December 23, 1999; Revised Manuscript Received February 7, 2000

ABSTRACT: Protein stability in vitro can be influenced either by introduction of mutations or by changes in the chemical composition of the solvent. Recently, we have characterized the thermodynamic stability and the rate of folding of the engineered dimeric leucine zipper A_2, which has a strengthened hydrophobic core [Dürr, E., Jelesarov, I., and Bosshard, H. R. (1999) *Biochemistry 38*, 870−880]. Here we report on the energetic consequences of a cavity introduced by Leu/Ala substitution at the tightly packed dimeric interface and how addition of 30% glycerol affects the folding thermodynamics of A_2 and the cavity mutants. Folding could be described by a two-state transition from two unfolded monomers to a coiled coil dimer. Removal of six methylene groups by Leu/Ala substitutions destabilized the dimeric coiled coil by 25 kJ mol^{-1} at pH 3.5 and 25 °C in aqueous buffer. Destabilization was purely entropic at around room temperature and became increasingly enthalpic at elevated temperatures. Mutations were accompanied by a decrease of the unfolding heat capacity by 0.5 kJ K^{-1} mol^{-1}. Addition of 30% glycerol increased the free energy of folding of A_2 and the cavity mutants by 5−10 kJ mol^{-1} and lowered the unfolding heat capacity by 25% for A_2 and by 50% for the Leu/Ala mutants. The origin of the stabilizing effect of glycerol varied with temperature. Stabilization of the parent leucine zipper A_2 was enthalpic with an unfavorable entropic component between 0 and 100 °C. In the case of cavity mutants, glycerol induced enthalpic stabilization below 50 °C and entropic stabilization above 50 °C. The effect of glycerol could not be accounted for solely by the enthalpy and entropy of transfer or protein surface from water to glycerol/water mixture. We propose that in the presence of glycerol the folded coiled coil dimer is better packed and displays less intramolecular fluctuations, leading to enhanced enthalpic interactions and to an increase of the entropy of folding. This work demonstrates that mutational and solvent effects on protein stability can be thermodynamically complex and that it may not be sufficient to only analyze changes of enthalpy and entropy at the unfolding temperature (T_m) to understand the mechanisms of protein stabilization.

Proteins fold to adopt unique spatial structures as a result of the energetic balance between intramolecular forces and interactions with the solvent. Since the net free energy of folding is small, the native state is populated within a narrow range of environmental parameters. Nevertheless, stability can be improved. Stabilizing mutations shift the midpoint of thermal transition to higher temperatures. Another way to increase thermal stability is to change the chemical composition of the solvent, an approach of obvious importance in pharmacology and biotechnology. Some organisms survive excess heat, dehydration, or accumulation of chemical substances by producing high amounts of low molecular weight protective compounds (*1*−*3*). Naturally occurring osmolytes such as amino acids, methylamines, sugars, polyols, and some salts are long known to effectively increase protein stability (*4*).

From a biophysical point of view, the main question is what are the energetic mechanisms underlying the change of protein stability in response to changes in the chemical composition of the solvent? In our current understanding, osmolytes, and other cosolvents are preferentially excluded from the immediate protein domain leading to preferential hydration of the protein. The model has been theoretically developed by Kirkwood, Kauzmann, Timasheff, and their colleagues and has been applied in numerous studies of protein/water/cosolvent systems (*5*−*8*). In general, the cosolvent perturbs the structure of water in such a way that the chemical potential of a protein increases in the mixed solvent relative to the potential in plain water. The effect is more pronounced for the unfolded state, which creates a larger cavity in the solvent structure than the folded state. To minimize this thermodynamically unfavorable situation, the polypeptide chain is forced to adopt its most compact conformation, which is usually the folded, native state (*7*, *9*).

Glycerol is one of the most extensively studied protein stabilizing agents. It is preferentially excluded from the protein hydration shell. Unlike sugars and kosmotropic salts,

† This work was supported in part by the Swiss National Science Foundation (Grant 3100-055308.98/1).

* To whom correspondence should be addressed. E-mail: iljel@bioc.unizh.ch. Fax: ++41 1 635 6805.

‡ Current address: The Scripps Research Institute, Departments of Molecular & Experimental Medicine and Vascular Biology, North Torrey Pines Road, La Jolla, CA 92037.

10.1021/bi992948f CCC: $19.00
Published on Web 03/24/2000

glycerol decreases the surface tension of water (*10*). The mechanism of glycerol effects on protein stability has been described in detail by Gekko and Timasheff, almost 20 years ago (*10*, *11*). An increase of the unfolding free energy in glycerol-containing solutions has been well documented for several globular proteins (*12*−*18*). A survey of the published work reveals no consistent picture on whether the glycerol effect is enthalpic, entropic, or both. Since glycerol often lowers but sometimes increases the unfolding heat capacity (ΔC_p^{unf}),[1] it follows that glycerol stabilization cannot be only enthalpic or only entropic if viewed over an extended range of temperatures. Here we have attempted to give a full thermodynamic description of the glycerol effect on the stability of a homodimeric coiled coil (leucine zipper). This is the first report on the energetics of glycerol-induced stabilization of a dimeric protein domain, which folds by association of unstructured polypeptide chains. Short naturally occurring or engineered leucine zippers are suitable models for experimental and theoretical studies of protein folding in vitro (*19*). Disordered amphiphilic peptide chains containing the recurring seven-residue motif **(abcdefg)**$_n$ fold together to form a stable coiled coil. The structure is stabilized mainly by hydrophobic packing of apolar side chains in positions **a** and **d** at the interhelical interface. We investigated how Leu/Ala substitutions in **d** positions change the thermodynamic properties at the hydrophobic core and how glycerol stabilization and cavity destabilization affect each other. The present work demonstrates how the folding of a leucine zipper is realized from a delicate balance between protein, low-molecular cosolutes, and solvent water.

EXPERIMENTAL PROCEDURES

Materials. All chemicals were of analytical grade substances and were used without further purification.

Peptide Synthesis and Purification. All peptides were synthesized by standard solid-phase synthesis protocols using the Rink amide MBHA resin (Novabiochem) and the 9-fluorenylmethyloxycarbonyl (N^{α}-Fmoc) protection strategy and were purified by reversed-phase high-performance liquid chromatography as described before in detail (*20*). Molecular mass of purified peptides was confirmed by electrospray mass spectroscopy. Concentrations were determined from UV-absorbance measurements in 6 M guanidinium hydrochloride using $\epsilon_{275.3nm} = 1450\ M^{-1}\ cm^{-1}$ (*21*).

Buffer. All experiments were conducted in a standard buffer composed of 7.5 mM each of phosphoric, citric, and boric acid adjusted to the desired pH with KOH or HCl and to a total ionic strength of 0.1 M with KCl. For preparation of glycerol-containing buffer, the pH was adjusted after glycerol addition. Reported pH values of glycerol-containing solutions are $pH = pH_{read} + 0.19$, where pH_{read} is the reading of a glass electrode at 25 °C. The glycerol concentration was verified by the freezing point method.

CD Spectroscopy. CD measurements were performed on a Jasco-715 spectropolarimeter equipped with a computer-controlled water bath, using thermostated cuvettes of 0.2 or 1 mm path length. Conformational changes induced by pH were monitored at 222 nm. Data were sampled for 3 min at 20 °C after preincubation of 25 μM peptide for 2−6 h at the desired pH. No further signal change was observed after 24 h incubation. Thermal unfolding curves were measured by continuously measuring the ellipticity at 222 nm between 3 and 90 °C at a scan rate of 0.8 deg min^{-1} and with data collection every 20 s. Reversibility of unfolding was checked by two cycles of heating and cooling or by following the time evolution of the CD signal for >1 h at a temperature close to the midpoint of spectral change and was always better than 95%.

Analysis of CD Data. Analysis of thermal unfolding curves and pH-induced unfolding curves followed the formalism describing a simple two-state conformational transition between folded coiled coil dimers, D, and unfolded random-coil monomers, M. At each temperature or pH, the observed molar ellipticity per residue, $[\theta]$, equals

$$[\theta] = f_M[\theta_M] + (1 - f_M)[\theta_D] \quad (1)$$

where f_M is the fraction of monomeric peptide and $[\theta_M]$ and $[\theta_D]$ are the molar ellipticities per residue of M and D, respectively. $[\theta_M]$ and $[\theta_D]$ were assumed to be linear functions of temperature or pH of the general form $[\theta_i] = [\theta_{i,0}] + \alpha_i T$ or $[\theta_i] = [\theta_{i,0}] + \alpha_i$pH, with i indicating M or D state. For a given total peptide concentration, C_{tot},

$$K_{unf} = \frac{2f_M^{\,2}C_{tot}}{1 - f_M} \quad (2)$$

from which f_M is calculated by

$$f_M = \frac{K_{unf}}{4C_{tot}}\left(\sqrt{1 + \frac{8C_{tot}}{K_{unf}}} - 1\right) \quad (3)$$

The unfolding enthalpy at the transition midpoint T_m ($f_M = 0.5$), ΔH_m, can be obtained from the temperature dependence of K_{unf} according to

$$K_{unf}(T) = C_{tot}\exp\left\{\frac{\Delta H_m}{R}\left(\frac{1}{T_m} - \frac{1}{T}\right) - \frac{\Delta C_p}{RT}\left[T - T_m - T\ln\left(\frac{T}{T_m}\right)\right]\right\} \quad (4)$$

R is the gas constant and ΔC_p is the heat capacity change. Equations 1−4 can be combined to analyze thermal unfolding curves by nonlinear curve optimization. In principle, the fitting yields ΔH_m, T_m, ΔC_p, $[\theta_{i,0}]$, and α_i. In practice, ΔH_m, T_m, and ΔC_p are strongly interdependent, and the statistical significance of fitting values extracted by analysis of a single trace is low. However, when ΔC_p is small, the second term in the wavy brackets in eq 4 is also small and can be neglected in the fitting. ΔC_p was obtained from a plot of ΔH_m vs T_m.

In a different treatment, $[\theta_M]$ and $[\theta_D]$ were defined by linear regression from the linear pretransitional and post-transitional parts of the CD trace to obtain a plot of $f_M = ([\theta] - [\theta_D])/([\theta_M] - [\theta_D])$ against T. From such plots ΔH_m was calculated as (*22*)

[1] Abbreviations: CD, circular dichroism; DSC, differential scanning calorimetry, ΔG_{unf}, unfolding free energy, ΔH_{unf}, unfolding enthalpy, ΔS_{unf}, unfolding entropy, ΔC_p^{unf}, unfolding heat capacity.

$$\Delta H_m = 6RT_m^2\left(\frac{\partial f_M}{\partial T}\right)_{T=T_m} \quad (5)$$

Results obtained by the two methods were identical within error.

Once ΔH_m, T_m, and ΔC_p are known, unfolding free-energy change, ΔG_{unf}, is calculated with help of the Gibbs−Helmholtz equation adapted to monomer−dimer equilibrium:

$$\Delta G_{unf}(T) = -RT \ln K_{unf}(T)$$
$$= \Delta H_m\left(1 - \frac{T}{T_m}\right) + \Delta C_p\left[T - T_m - T\ln\left(\frac{T}{T_m}\right)\right] - RT \ln K_{unf}(T_m) \quad (6)$$

K_{unf} (T_m) = C_{tot} in the case of homodimeric systems.

Molar ellipticity changes observed in pH titrations were first transformed to plots of $f_M = ([\theta] - [\theta_D])/([\theta_M] - [\theta_D])$ against pH. Lines shown in Figure 2 were calculated by a modified form of the Hill equation (*23*):

$$f_M = \frac{10^{n(pH-pK)}}{1 + 10^{n(pH-pK)}} \quad (7)$$

p*K* is the pH at the midpoint of the pH-induced transition, and *n* is the steepness of the transition. Values of $n \approx 2$ were found in all experiments indicating high cooperativity. The number of protons taken up when the leucine zipper folds at a given pH was calculated from (*24*)

$$\Delta\nu = \frac{\partial \ln K_{unf}}{\partial \ln[H^+]} \quad (8)$$

Differential Scanning Calorimetry. DSC experiments were performed on the VP-DSC microcalorimeter (MicroCal Inc.) equipped with twin coin-shaped cells of 0.52 mL volume. Technical details and performance of the instrument have been described (*25*). Peptides were dialyzed for 18−24 h against the same batch of buffer used to establish the baseline. The scan rate was 1 deg min^{-1}. Reversibility was checked by two to four cycles of heating and cooling and was better than 95%.

Analysis of DSC Data. It was difficult to define accurately the pretransitional and posttransitional parts of the heat capacity traces recorded in glycerol-containing solutions. Therefore, since ΔC_p was much smaller than the height of the heat capacity peak, $\langle C_p\rangle_{max}$, and for the purpose of comparison, only the excess heat capacity function, $\langle C_p\rangle^{ex}$, was analyzed. To do this, the linear portions of the trace preceding and following the main transition peak were connected with a third-order spline function, and the resulting baseline was subtracted from the experimental data. The unfolding enthalpy was calculated in three ways. (i) The calorimetric, model-independent enthalpy, ΔH(cal), was obtained by integration of $\langle C_p\rangle^{ex}$. (ii) The effective van't Hoff enthalpy, ΔH(vH), was calculated according to (*26*)

$$(\sqrt{n} + 1)T_m\sqrt{R\left[\langle C_p\rangle_{max} - \frac{\Delta C_p\sqrt{n}}{(\sqrt{n} + 1)}\right]} \quad (9)$$

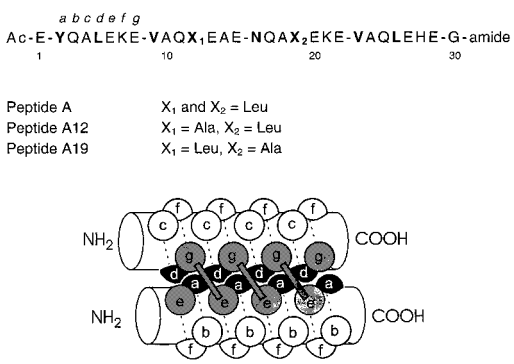

FIGURE 1: Sequence of peptides A, A12, and A19 and schematic structure of the parallel two-stranded leucine zippers A_2, $(A12)_2$, and $(A19)_2$. Sequences: hydrophobic residues in heptad positions *a* and *d* are in bold; heptads are separated by hyphens. Schematic 3D-structure: each strand of the parallel coiled coil is drawn as a rod with the approximate position of the side chains indicated by spheres. Heptad positions are lettered; positions *a* and *d* are in dark gray and positions *g* and *e* in light gray. Interhelical electrostatic repulsions between Glu's in *e* and *g* positions are indicated. Peptides A_2, $(A12)_2$, and $(A19)_2$ formed at low pH where glutamate side chains became protonated.

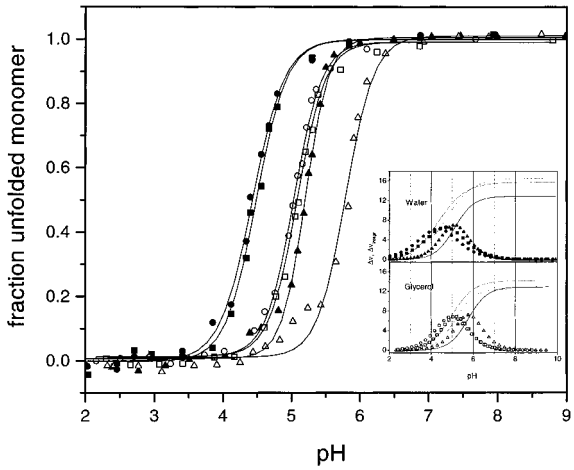

FIGURE 2: pH dependence of the conformational equilibrium between unfolded monomer and folded dimer at 20 °C. Measurements were made with 25 μM peptid A (triangles), peptide A12 (squares), and peptide A19 (circles). Filled symbols represent measurements in plain buffer, open symbols in 30% (w/w) glycerol. Continuous lines are fits according to eq 7. (Inset) Symbols, $\Delta\nu$; lines, $\Delta\nu_{integr}$. Solid line, A; dotted line, A12; dashed line, A19. Upper panel, experiments in buffer; lower panel, experiments in 30% (w/w) glycerol. $\Delta\nu$ = number of protons taken up on folding at a given pH. $\Delta\nu_{integr}$ = total number of protons for full protonation of the coiled coil at a given pH.

with ΔC_p set to zero and $n = 2$ for a bimolecular transition. (iii) The validity of the two-state model of unfolding accompanied by subunit dissociation was tested by nonlinear regression analysis of $\langle C_p\rangle^{ex}$ according to the following equation as implemented in the data analysis software of the instrument and modified to account for the fact that the intrinsic change in heat capacity had been subtracted prior to analysis:

$$\langle C_p\rangle^{ex} = \frac{\Delta H^2}{RT^2}\left[\frac{f_M(1 - f_M)}{n - f_M(n - 1)}\right] \quad (10)$$

n is the number of peptide chains and f_M can be numerically solved from

$$K_{unf} = \frac{f_M{}^n\, n^n A_{tot}{}^{n-1}}{1 - f_M} \quad (11)$$

where A_{tot} is the total concentration of *n*-mers and $K_{unf}(T)$ is calculated with reference to $T_{m0.5}$ ($f_M = 0.5$) by

$$K_{unf}(T) = 0.5^{n-1}\, n^n A_{tot}{}^{n-1} \exp\left[-\frac{\Delta H}{RT}\left(1 - \frac{T}{T_{m0.5}}\right) - \frac{\Delta C_p}{RT}\left(T - T_{m0.5} - T \ln \frac{T}{T_{m0.5}}\right)\right] \quad (12)$$

Fits were also performed according to a formalism with explicit specification of the stoichiometry of unfolding transition as proposed in (*27*)

$$\langle Cp \rangle = C_p{}^N + \Delta C_p \frac{Q-1}{Q+1} + \frac{\Delta H^2}{RT^2} \frac{2Q(Q-1)}{(Q+1)^3} \quad (13)$$

with *Q*, the partition function, being defined as

$$Q = \frac{2D + M}{2D} = 1 + \frac{2}{\sqrt{1 + \frac{8C_{tot}}{K_{unf}}} - 1} \quad (14)$$

Results obtained by application of the combined eqs 10−12 (*n* was floating parameter) or by the combined eqs 13−14 were the same.

Error Analysis. Errors in thermodynamic functions derived from fitted parameters were estimated from the variance. The variances in $\Delta H_{unf}(T)$ and $\Delta G_{unf}(T)$ are given, respectively, by

$$\sigma_{\Delta H} = \sigma_{\Delta H_m}{}^2 + \sigma_{\Delta C_p}{}^2 (T - T_m)^2 + \sigma_{T_m}{}^2 \Delta C_p{}^2 \quad (15a)$$

and

$$\sigma_{\Delta G} = \sigma_{\Delta H_m}{}^2 (1 - T/T_m)^2 + \sigma_{\Delta C_p}{}^2 [(T - T_m - T \ln (T/T_m)]^2 + \sigma_{T_m}{}^2 [\Delta C_p (T/T_m - 1) + \Delta H_m T/T_m{}^2]^2 + \sigma_{C_{tot}}{}^2 (RT/C_{tot})^2 \quad (15b)$$

The error of ΔH_m ($\sigma_{\Delta H_m}$) from CD experiments was estimated as follows. For each individual melting curve, ΔH_m was calculated according to eqs 1−4 with the slopes of the pretransition baseline, posttransition baseline, or both at the same time, being either free-floating or fixed parameters. Since there was no statistically significant trend for the slopes to vary with pH and peptide concentration, the slopes were fixed either as the mean slope of the entire data set collected at identical buffer composition or as the mean slope observed at the same pH and buffer conditions. This procedure resulted in 6−10 values of ΔH_m, from which a standard deviation of 8−15 kJ mol^{-1} (5−10% of the mean, depending on the mean ΔH_m) was calculated.

Linear fit of ΔH_m vs T_m (Figure 4) resulted in a fitting error of $\Delta C_p{}^{unf}$ of the order of 0.1 kJ K^{-1} mol^{-1}. A more reliable estimate of $\sigma_{\Delta C_p}$, 0.2 kJ K^{-1} mol^{-1}, was obtained by systematic truncation of the data by one point at a time. The terms including errors in T_m and C_{tot} could be neglected since the error in T_m was <1 K and the error in C_{tot} was <10%.

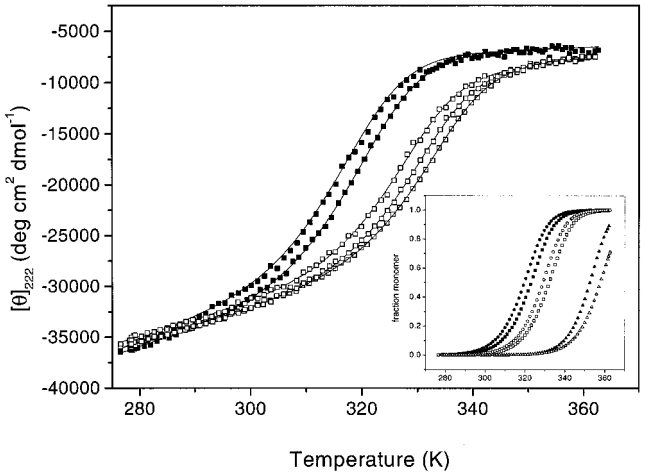

FIGURE 3: Thermal unfolding of leucine zipper $(A12)_2$ monitored by CD. Melting at pH 3.5 of 27 and 52 μM peptide in plain buffer (filled squares, left to right) and of 27, 54, and 100 μM peptide in 30% (w/w) glycerol (open squares, left to right). Solid lines are best fits according to eqs 1−4 describing two-state unfolding. (Inset) Normalized melting curves for A_2 (triangles), $(A12)_2$ (squares), and $(A19)_2$ (circles). Data collected for 100 μM peptide at pH 3.5 are presented as fraction monomer calculated according to eq 3. Filled symbols, plain buffer; open symbols, 30% (w/w) glycerol.

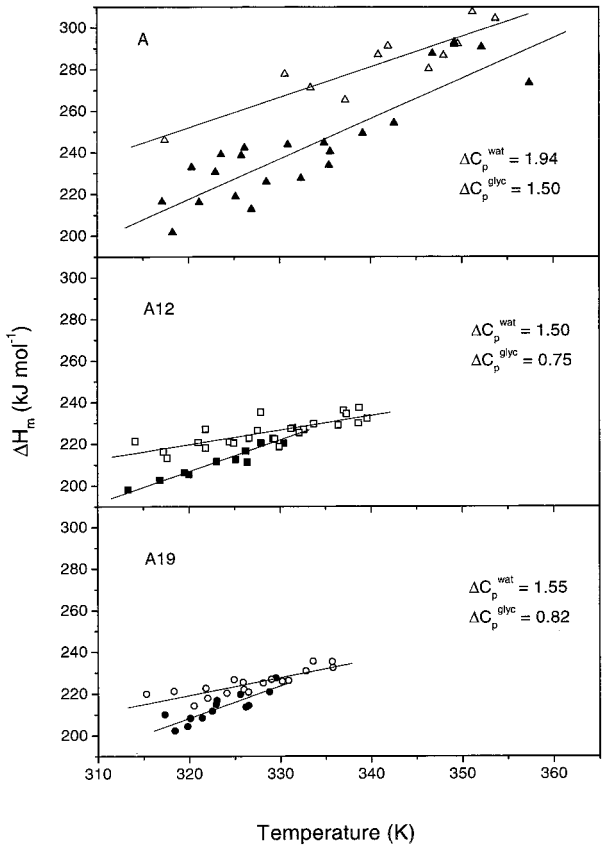

FIGURE 4: Van't Hoff analysis of CD thermal unfolding experiments performed in the pH range 2−4.9 and with peptide concentrations from 6 to 500 μM (data from Tables 1, 2, and 3). Triangles, peptide A; squares, peptide A12; circles, peptide A19. Filled symbols, plain buffer; open symbols, 30% (w/w) glycerol. Solid lines are linear best fits from which the heat capacity change in plain buffer, ΔC_p^{wat}, and in 30% (w/w) glycerol, ΔC_p^{glyc}, were calculated. Errors of ΔC_p are on the order of 0.2 kJ K^{-1} mol^{-1} (see Error Analysis in Experimental Procedures).

According to eqs 15a and 15b and using $\sigma_{\Delta C_p}$ and $\sigma_{\Delta H_m}$ obtained as explained above, the maximal errors in ΔH_{unf}-

(T) and $\Delta G_{unf}(T)$ were 20 kJ mol^{-1} and 3.5 kJ mol^{-1}, respectively, for the longest extrapolation away from T_m. Maximal errors in $\Delta\Delta H_{unf}(T)$ and $\Delta\Delta G_{unf}(T)$ were, therefore, 25 and 5 kJ mol^{-1}, respectively. Values of $T\Delta S_{unf}(T)$ and $T\Delta\Delta S_{unf}(T)$, calculated from ΔH_{unf} and ΔG_{unf} contained the same uncertainty on the order of 20−25 kJ mol^{-1}. Usually the errors in the calculated thermodynamic parameters at a given temperature were smaller than these maximal values, since extrapolations were shorter.

RESULTS

Structure of Peptides. The sequences of the three peptides used in this study are shown Figure 1. Peptide A had the pattern $L^dV^aL^dN^aL^dV^aL^d$ of hydrophobic residues in positions **a** and **d**. This pattern was derived from the leucine zipper domain of the natural transcription factor GCN4 and favors formation of a parallel and in-register dimeric coiled coil (*28*, *29*). In the first **a** position a Tyr was introduced to facilitate concentration determination by UV spectroscopy. Helix-stabilizing residues were selected for positions **b**, **c**, and **f** located on the solvent-exposed surface of the coiled coil. Two **f** positions were occupied by Lys and one by His to keep the peptides soluble at low pH. Peptides A12 and A19 had a single Leu/Ala replacement in position **d**12 and **d**19, respectively, which created a cavity at the dimer interface. The peptides had a negative charge of −7e at neutral pH.

In recent work, we have shown by ultracentrifugation, CD spectroscopy, and DSC experiments that peptide A is monomeric and adopts a random coil conformation at neutral pH but forms a stable dimeric coiled coil below pH 5 (*30*). The coiled coil also forms above pH 5 in the presence of kosmotropic salts (*31*). A combined kinetic and thermodynamic approach has demonstrated unfolded monomer, A, and folded dimer, A_2, to be the only species detectably populated under various buffer conditions and concentrations up to 500 μM concentration.

Acid-Induced Folding. At neutral pH and in aqueous buffer, the CD spectra of the three peptides were identical and typical of a random coil conformation. Helical content progressively increased when the pH was lowered (Figure 2). Below pH 3.5, spectra typical of an α-helical conformation were recorded, with minima at 208 and 222 nm and with $[\theta]_{222} = -37\,000$ deg cm^2 dmol^{-1} at 0 °C accounting for nearly 100% helix content. The sharp pH-induced conformational transition was completed within 1 pH unit with midpoints at pH 5.2, 4.5, and 4.4 for peptides A, A12, and A19, respectively (Figure 2). There was no alteration of the CD spectral features upon addition of glycerol except that the midpoints of the coil-to-helix transition were shifted by 0.6 pH units to higher values. The transition half-width remained unchanged. Therefore, glycerol appeared to stabilize the coiled coil conformation at room temperature.

Data from the main plot of Figure 2 were used to calculate the unfolding equilibrium constant, K_{unf}, and $\Delta\nu$, the number of protons taken up in folding (closed and open symbols in inset of Figure 2). Integration of $\Delta\nu$ yielded $\Delta\nu_{integr}$, the number of protons necessary to completely protonate the peptide at a given pH (lines in inset of Figure 2). The maximum value of $\Delta\nu_{integr}$ was 13 protons/dimer of A_2. This means that on transition from pH >8 to about pH ∼2, the formation of A_2 from two unfolded peptide chains was accompanied by uptake of 13 protons. Addition of 30% glycerol did not change this number. Formation of $(A12)_2$ and $(A19)_2$ involved a maximum of 14−16 protons in plain buffer and 12−14 protons in the presence of 30% glycerol. More unfavorable charge−charge repulsions had to be eliminated to form the leucine zippers with a cavity. Addition of glycerol tended to relax this requirement.

Thermal Denaturation Followed by CD. The influence of glycerol on the energetics of folding below pH 5 was investigated by thermal unfolding experiments. The CD spectra of the three peptides showed a typical loss of α-helical content when the temperature was raised, with a well-defined isodichrioc point at 203 nm indicative for a two-state process. Thermal unfolding was reversible to >95% at all concentrations and pH values tested. Figure 3 shows examples of CD unfolding curves for peptide A12 and illustrates the common features observed for all three peptides under study. (i) Increasing the peptide concentration shifted the transition midpoint to higher temperature, as expected for a system undergoing unfolding from an oligomeric folded state to a monomeric denatured state. Addition of glycerol did not alter this behavior. (ii) When the water activity was lowered by adding glycerol, the transition midpoint at identical peptide concentration shifted to higher temperature. (iii) The helical content extrapolated to the lowest and highest experimentally accessible temperatures, 3 and 95 °C, respectively, was not influenced by the addition of glycerol. (iv) The slope of the posttransitional linear segment of the melting trace was steeper in the presence glycerol; for the entire set of data, $\partial[\theta]_{222}/\partial T = 28 \pm 5$ deg cm^2 dmol^{-1} K^{-1} in buffered water and $\partial[\theta]_{222}/\partial T = 65 \pm 10$ deg cm^2 dmol^{-1} K^{-1} in 30% glycerol. The significance of this last observation is not clear. However, if $[\theta]_{222}$ of the folded and the denatured states are linear functions of the temperature as commonly assumed, the difference $\Delta[\theta]_{222} = [\theta]_{222}^{fold} - \Delta[\theta]_{222}^{unf}$ was smaller at all temperatures when glycerol was added to the system.

The solid lines in Figure 3 are best fits based on the combined eqs 1−4, which describe a two-state equilibrium between folded dimer and unfolded monomer. Values of T_m and ΔH_m are summarized in Tables 1, 2, and 3 (Supporting Information), and plots of ΔH_m vs T_m are shown in Figure 4. Variation of peptide concentration and pH allowed the collection of data in an interval of 15−25 °C for A12 and A19 and over a range of nearly 45 °C for peptide A. The heat capacity changes accompanying thermal unfolding, ΔC_p^{unf}, were obtained from the slopes of the regression lines and are included in Figure 4. ΔC_p^{unf} of $(A12)_2$ and $(A19)_2$ was the same within error and was ∼25% smaller than ΔC_p^{unf} of A_2. Glycerol reduced ΔC_p^{unf}. The reduction was larger for the cavity-containing leucine zippers.

Thermal Denaturation Followed by DSC. Calorimetric experiments were performed with 300 μM peptide at pH 3.5 in the presence and absence of glycerol. Thermal unfolding was nearly fully reversible even after three consecutive cycles of heating and cooling. As already demonstrated by CD, addition of glycerol shifted T_m by 8−10 °C to higher temperature. Since the pretransitional and posttransitional heat capacities measured in glycerol were ill defined, only the excess heat capacity traces were analyzed as shown in Figure 5. The excess heat capacity peaks were broad and

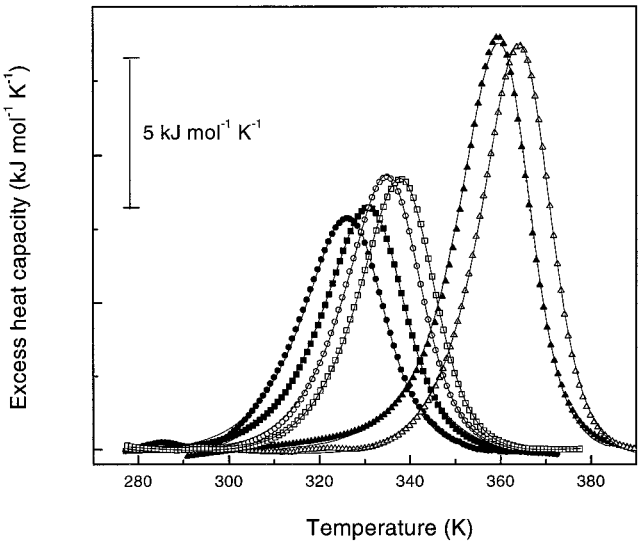

FIGURE 5: Excess molar heat capacities of peptide A (triangles), A12 (squares), and A19 (circles). DSC experiments were made at pH 3.5 with 300 μM total peptide concentration at scanning rate of 1 deg min^{-1}. Symbols are experimental data collected in buffer with or without addition of glycerol (open and filled symbols, respectively). Solid lines are fits to a two-state unfolding transition accompanied by dissociation (see Experimental Procedures for details).

asymmetric. The maximum excess molar heat capacity was at temperatures corresponding to 0.57−0.59 of the maximal heat absorption, an independent proof of an unfolding reaction linked to a bimolecular dissociation event. The data were well described by nonlinear regression fits according to eqs 10−15. Best fits were obtained for $n = 2.1 \pm 0.1$ (eqs 10−12). The ratio $\Delta H_{cal}/\Delta H_{vH}$ was 0.9−0.94. The good correspondence between enthalpies calculated by statistical thermodynamic procedures, by simple van't Hoff considerations and by direct integration of the excess heat absorption peak, strongly supports the conclusion that addition of glycerol does not perturb the molecular mechanism of thermal unfolding.

Temperature and pH Dependence of Thermodynamic Functions. T_m, ΔH_m, and ΔC_p^{unf} were used to calculate the temperature dependence of the unfolding free energy, ΔG_{unf}, the unfolding enthalpy, $\Delta H_{unf,}$ and the unfolding entropy, ΔS_{unf}, as a function of temperature in plain buffer and in glycerol-containing buffer (eq 6). Figure 6 shows a comparison of the thermodynamic functions of the peptides at pH 3.5. Pairs of T_m and ΔH_m in the middle of the experimental temperature range (regression lines in Figure 4) were used in the calculation. The entropy-related part of ΔG_{unf} was calculated from $T\Delta S_{unf} = \Delta H_{unf} - \Delta G_{unf}$. In the plots, $T\Delta S_{unf}$ instead of ΔS_{unf} is presented to ease comparisons between the magnitudes of enthalpic and entropic contributions to ΔG_{unf}. ΔS_m could also be estimated from DSC experiments by integrating the excess heat capacity peak in respect to ln T. Values of $T\Delta S_m$ calculated in this were within 10% of $T\Delta S_{unf}$, indicating that the errors in entropy and enthalpy were of the same magnitude.

In Figure 7, the stability curves in the range pH 2−6 are shown. The figure combines results from thermal unfolding and pH titration. Combined ΔG_{unf} values fit together nicely and demonstrate glycerol stabilization in the entire pH range studied.

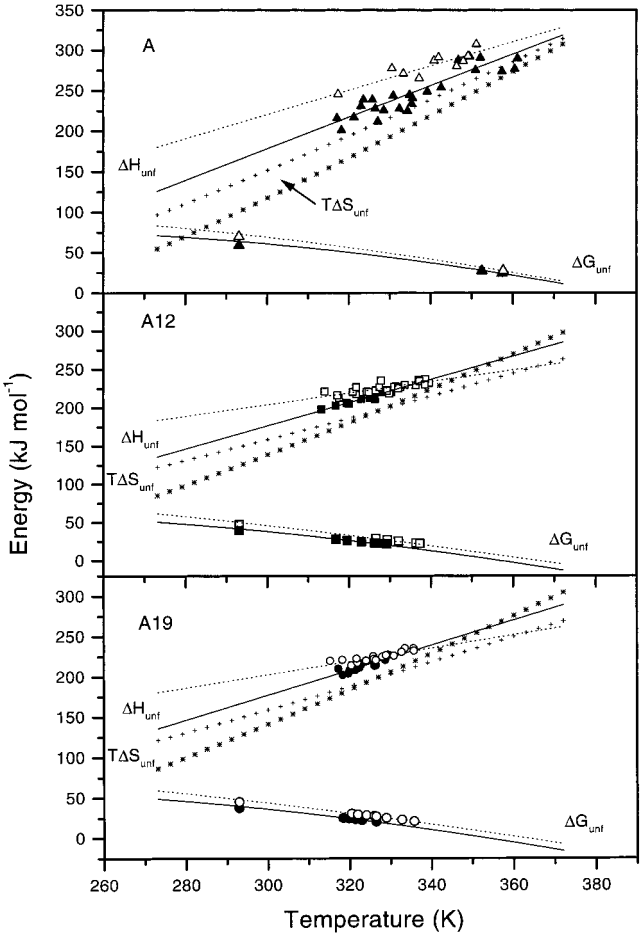

FIGURE 6: Thermodynamic stability profiles at pH 3.5. Filled symbols and continuous lines, experimental data and calculated functions in plain buffer; open symbols and dotted lines, experimental data and calculated functions in 30% (w/w) glycerol. Stars, $T\Delta S_{unf}$ in plain buffer; crosses, $T\Delta S_{unf}$ in 30% (w/w) glycerol. $\Delta G_{unf}(T)$ calculated by eq 6. $\Delta H_{unf}(T) = \Delta H(T_m) + \Delta C_p(T - T_m)$. $T\Delta S_{unf} = \Delta H_{unf}(T) - \Delta G_{unf}(T)$. See Experimental Procedures for details in error analysis.

To visualize the thermodynamic changes caused by a cavity at the hydrophobic core and by adding glycerol over the range 0−100 °C, we calculated values of $\Delta\Delta E_{unf}$ as follows:

$$\Delta\Delta E_{unf} = \Delta E_{unf}^{mut} - \Delta E_{unf}^{A} \quad (16)$$

$$\Delta\Delta E_{unf} = \Delta E_{unf}^{glyc} - \Delta E_{unf}^{wat} \quad (17)$$

$\Delta E = \Delta G$, ΔH, or $T\Delta S$. The superscripts refer to the peptide (mut = A12 or A19) or to the presence (glyc) or absence (wat) of glycerol. Figure 8 shows the data plotted according to eq 16 in the absence and in the presence of glycerol. Destabilization by a single Leu/Ala substitution led to a very similar $\Delta\Delta G_{unf}$ in the entire temperature range and independent of the presence or absence of glycerol. However, partition of the destabilizing effect into its enthalpic and entropic components differed markedly. In plain buffer, destabilization was caused by a higher unfolding entropy up to high temperatures ($T\Delta S_{unf} > 0$). At low temperature, the cavity mutants were enthalpically even more stable than the parent leucine zipper A_2 ($\Delta\Delta H_{unf} > 0$). Thus, destabilization changed from being mainly entropic at low temperature to

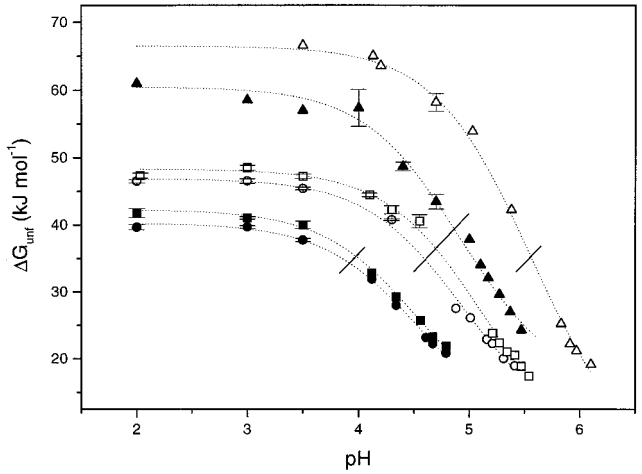

FIGURE 7: pH-dependent stability of peptide A (triangles), A12 (squares), and A19 (circles). Filled symbols, ΔG_{unf} in plain buffer; open symbols, ΔG_{unf} in 30% (w/w) glycerol. Dotted lines are smooth spline functions connecting the data points and have no physical meaning. Slanting lines demarcate data from different types of experiments. Points to the left and above the lines are mean ΔG_{unf} from CD thermal unfolding experiments made at the corresponding pH with different peptide concentrations and were calculated by eq 6. Points to the right and below the lines were calculated by $\Delta G_{unf}(\text{pH, 293 K}) = -293.15R \times \ln K_{unf}(\text{pH, 293 K})$ with the data shown in Figure 2 and K_{unf} obtained from eq 2.

being mainly enthalpic at elevated temperature, with a switch around 50 °C ($|\Delta H_{unf}| = |T\Delta S_{unf}|$). This lead to almost perfect enthalpy−entropy compensation and, therefore, to almost constant $\Delta\Delta G_{unf}$ in the entire temperature range. In the presence of glycerol, the picture was, in principle, the same. But now the switch from mainly entropic destabilization to mainly entropic stabilization occurred already around 18 °C. Glycerol decreased the isoenthalpic temperature ($\Delta\Delta H_{unf} = 0$) by about 20 °C and the isoentropic temperature ($T\Delta\Delta S_{unf} = 0$) by nearly 50 °C.

A similar shift in enthalpic and entropic stabilization was seen if one compared the effect of glycerol on the parent leucine zipper A_2 and on the cavity mutants $(A12)_2$ and $(A19)_2$ (Figure 9; only the data for $(A12)_2$ are presented since both mutants showed essentially the same behavior). Stabilization of leucine zipper A_2 by glycerol was enthalpic from 0 to 100 °C. In contrast, stabilization of the cavity mutants switched from enthalpic below 50 °C to entropic above 50 °C. The isoentropic and isoenthalpic temperatures ($\Delta\Delta H_{unf} = 0$, $T\Delta\Delta S_{unf} = 0$) were 40−50 °C lower for the mutant leucine zippers

DISCUSSION

Thermodynamic Destabilization of Coiled Coil Structure by Cavity Mutations. Previously, we have performed a combined thermodynamic and kinetic analysis of the homodimer A_2, which is formed by protonation-induced association of two 30-residues long acidic peptide chains (*30*). In the present work, we have characterized the folding energetics of two variants of A_2 with a cavity in the hydrophobic core. The general architecture and the folding mechanism of the mutants were not significantly perturbed by the Leu/Ala substitution. Their overall thermodynamic behavior closely resembled that of the leucine zipper A_2. For each peptide, ΔH_{unf}, T_m, and the steepness of the unfolding transition were the same within error in CD and

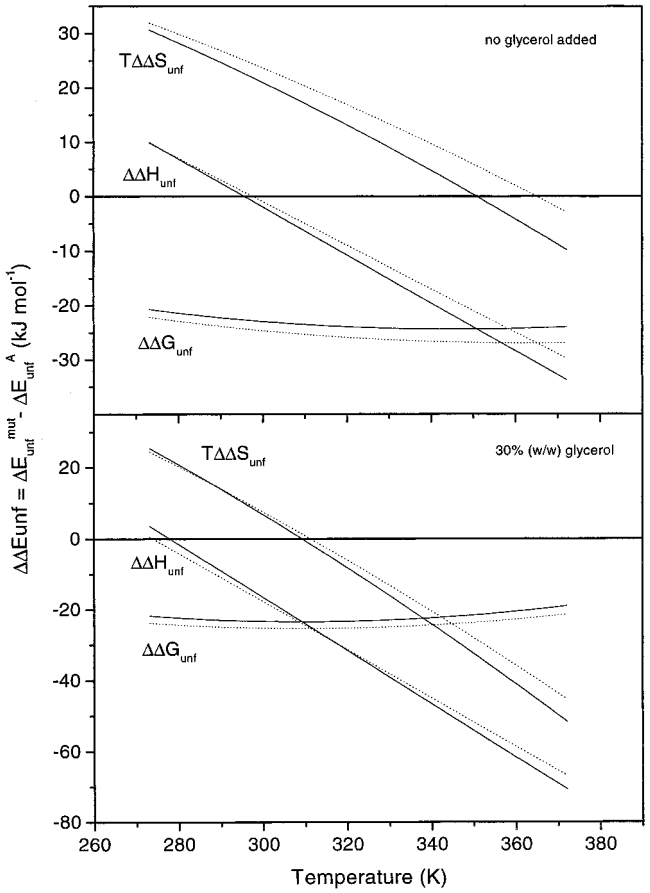

FIGURE 8: Changes in thermodynamic unfolding parameters caused by cavity mutation. $\Delta\Delta E_{unf}$ was calculated according to eq 16, using folded dimer A_2 as the standard state. Destabilization by the cavity mutation is indicated by $\Delta\Delta G_{unf} < 0$, $\Delta\Delta H_{unf} < 0$, and $T\Delta\Delta S_{unf} > 0$. Solid lines, cavity mutant $(A12)_2$; dotted lines, cavity mutant $(A19)_2$; top panel, stability curves in plain buffer, pH 3.5; bottom panel, stability curves in the presence of 30% (w/w) glycerol, pH 3.5.

DSC experiments. Therefore, the loss of secondary structure (CD) and the disruption of packing interactions (DSC) occurred simultaneously. A rigorous analysis of heat capacity traces indicated that only the unfolded monomer and folded dimer were noticeably populated. Finally, the relative populations of dimer and monomer changed with almost identical cooperativity upon lowering of pH at room temperature. Together, these observations strongly indicate that the changed thermodynamic parameters measured for the cavity mutants could be ascribed to the disruption of the hydrophobic core.[2]

Cavity-induced destabilization lowered the midpoint pH of acid-induced folding (Figure 2). Since there was no reason to assume that the Leu/Ala substitution perturbed the intrinsic pK_a of side-chain carboxyl groups, we expected that more negative charges had to be eliminated in order to compensate for the lower stability of $(A12)_2$ and $(A19)_2$. This was indeed the case. About 16 protons were taken up by peptides A12 and A19, and only about 13 protons were taken by peptide

[2] We used AGADIR to predict the amount of helix present in the monomeric peptides (*32*). At 25 °C, pH between 2 and 4.3 and 0.1 ionic strength the predicted helical content of peptides A, A12, and A19 is 5−6%. Hence, based on the AGADIR calculation, the amount of potential helical monomer was negligible already at temperatures where the native dimeric state was almost 100% populated.

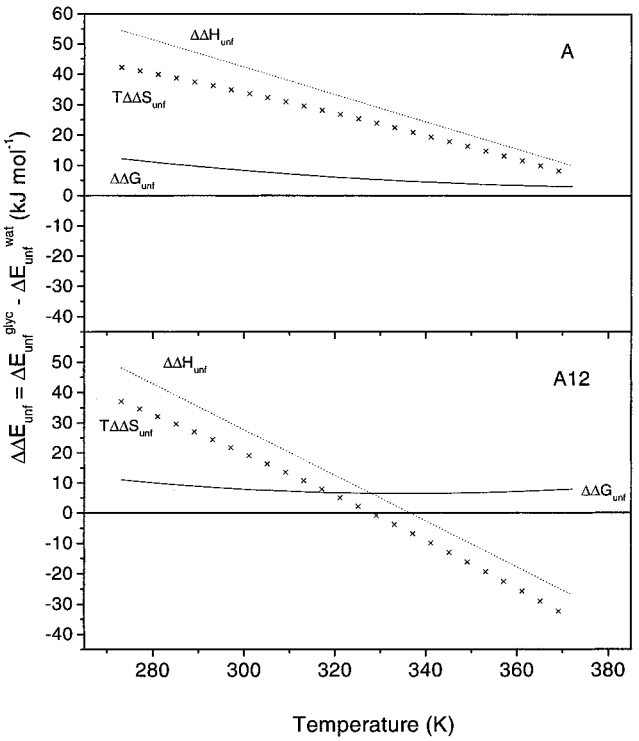

FIGURE 9: Glycerol-induced changes in the thermodynamic unfolding parameters of leucine zipper A_2 (top) and $(A12)_2$ (bottom). $\Delta\Delta E_{unf}$ was calculated according to eq 17, using the folded leucine zipper in plain buffer, pH 3.5, as the standard state. Stabilization by 30% (w/w) glycerol is indicated by $\Delta\Delta G_{unf} > 0$, $\Delta\Delta H_{unf} > 0$, and $T\Delta\Delta S_{unf} < 0$.

A on folding in the pH interval 8−2 ($\Delta\nu_{integr}$ in inset of Figure 2). Expressed differently, peptide A was 80% folded at pH 5 after taking up seven protons. At the same pH and after taking up the same number of protons, peptides A12 and A19 were only 10% folded ($\Delta\nu$ in inset of Figure 2). Strong destabilization was also reflected by a 30 °C shift of T_m (Figure 3, inset).

In comparing A_2 with the cavity mutants one notes that overall destabilization caused by the Leu/Ala substitution, expressed as $\Delta\Delta G_{unf}$, was of similar magnitude from 0 to 100 °C. Destabilization was also virtually independent of pH (Figure 7). Dissection of $\Delta\Delta G_{unf}$ into $\Delta\Delta H_{unf}$ and $T\Delta\Delta S_{unf}$ revealed a complex pattern (Figure 8, upper panel). Destabilization was mainly entropic at temperature lower than 50 °C and became increasingly enthalpic at higher temperature.

It is not easy to rationalize the cavity-induced destabilization in structural terms. It has been argued that a cavity in the core of a protein created by removal of methylene groups destabilizes the folded state primarily through loss of favorable packing interactions (*33*, *34*). This effect is expected to lower ΔH_{unf} since the enthalpy of transfer of nonpolar groups from the protein interior to water is positive at elevated temperature (*35*). As the temperature decreases, the enthalpic contributions of van der Waals interactions and apolar hydration tend to cancel and destabilization caused by removal of buried aliphatic groups changes from enthalpic to entropic, exactly as observed in the present study. Furthermore, the negative entropy of apolar hydration could explain to some extent why our mutants, which expose less apolar surface upon unfolding, were entropically destabilized ($T\Delta\Delta S_{unf} > 0$) and why the heat capacity change was lower. Calorimetric data on thermal unfolding of isolated α-helices and dimeric coiled coils have demonstrated that the enthalpic contribution of nonpolar groups to stability vanishes at 25 °C and that the total unfolding enthalpy at that temperature can be assigned to disruption of hydrogen bonds and hydration of polar groups (*36*). The changes in unfolding enthalpy and unfolding entropy of the core mutants studied here are, therefore, not only in good correspondence to predictions based on transfer data but also confirm direct experimental estimates for related systems in a protein context.

Comparison with Leu/Ala Substitution in Electrostatically Stabilized Leucine Zippers. Previously, we had studied Leu/Ala mutations in the heterodimeric leucine zipper AB, which is closely related to the homodimeric leucine zippers studied here. AB contained the acidic chain A and the basic chain B, the latter having Lys in all the **e** and **g** positions (*37*). AB was electrostatically stabilized because of its oppositely charged residues in **e** and **g** (*20*). Leu/Ala substitutions in A12B and A19B, as well as in AB12 and AB19 (nomenclature analogous to present work), produced a net decrease in overall stability of less than 2 kJ mol^{-1}/methylene group as compared to 3−4 kJ mol^{-1}/methylene group observed here for $(A12)_2$ and $(A19)_2$. Furthermore, Leu/Ala substitution did not change ΔC_p^{unf} of the heterodimeric AB-type leucine zipper, which was 4 kJ mol^{-1} K^{-1}, more than twice ΔC_p^{unf} observed here for A_2 and its cavity mutants. We can only speculate about the reasons for the different effect of a Leu/Ala substitution on two leucine zippers that have the same sequence except for the charged residues in **e** and **g** positions. The heterodimeric AB zipper is most stable at neutral pH values where its peptide chains are oppositely charged. Hence, the water-exposed surface of folded AB is much more polar than the surface of A_2 at acidic pH, where most negative charges are neutralized. Uncharged Glu residues strengthen the hydrophobic shielding of the coiled coil interior, possibly leading to a better packing of the core (*30*, *38*). Electrostatic interactions in AB may impose strain on the helical backbone, which could lead to suboptimal packing interactions in the hydrophobic core. Hence, better packing and increased backbone flexibility of folded A_2 in the folded state could explain the larger destabilization introduced by a cavity in this coiled coil.

In summarizing the discussion on the effect of a cavity mutation on leucine zipper stability, we note that the origin of the destabilization changed with temperature in a conspicuous way, which can be rationalized, at least in qualitative terms, by changing contributions of van der Waals interactions and apolar and polar hydration to the overall stability. Moreover, cavity effects may not only depend on local structure but also on local dynamics as seen when the present results are compared to cavity mutations in a related but electrostatically stabilized leucine zipper.

Glycerol Effect on Overall Stability. Addition of glycerol stabilized A_2 and its mutants, as manifested by higher T_m's of thermal unfolding (Figure 3) and by higher pH midpoints of the protonation-induced coil-to-helix transitions (Figure 2). The slopes of the transitions measured by CD in the presence and absence of glycerol were very similar (Figure 3) as were the shapes of the excess heat capacity traces (Figure 5). Hence, decreasing the water activity did not change the folding mechanism; the cosolvent merely influenced the energetics of folding.

The three zippers were stabilized by $\Delta\Delta G_{unf} = 5-10$ kJ mol^{-1}, slightly depending on the temperature (Figure 9). $\Delta\Delta G_{unf}$ of such magnitude has been typically observed for other proteins in the presence of glycerol or other polyols (*11*, *17*). The closely related 30-residue long leucine zipper of the transcription factor GCN4 was stabilized by 8.5 kJ mol^{-1} in 15.2% glycerol at neutral pH and 25 °C (*39*). Interestingly, glycerol increased the stability of A_2 and its mutants to the same extent despite that cavity mutants were 20−25 kJ mol^{-1} less stable. The stabilization effect of glycerol showed no detectable pH dependence in the range 2−5.5, where the free energy of unfolding displays a broad variation (Figure 7). These observations and results for other proteins of very different size, molecular architecture, and stability indicate that the glycerol effect is of rather nonspecific nature (*8*).

It is generally thought that stabilization by glycerol follows the preferential exclusion of the cosolvent from the protein domain, resulting in preferential hydration of the solvent exposed molecular surface. Preferential hydration raises the chemical potential of both the native and the denatured state in water/glycerol mixtures relative to pure water. Since the change in chemical potential scales with the amount of solute−solvent contacts, the folded conformation, with a large proportion of molecular surface buried in the protein interior, is thermodynamically favored. However, preferential hydration does not mean that the cosolvent may not penetrate the solvation shell of the protein. Glycerol has a hydrophilic character and can effectively interact with water molecules, thus strengthening the solvent structure around the protein. Indeed, the amount of glycerol in the immediate vicinity of several proteins has been found to be a nonzero quantity (*10*, *17*). Moreover, preferential hydration decreases in magnitude as the polar character of the protein increases (*10*, *40*). Therefore, it may seem surprising that $\Delta\Delta G_{unf}$ did not change between pH 5.5 and pH 2 (Figure 7) despite that the polar character of the coiled coil surface decreased when more Glu side chains were protonated in the folded leucine zipper. The polar contribution to the preferential hydration thermodynamics was thus either not large or, else, compensated by other effects.

Glycerol Effect on ΔH_{unf}, ΔS_{unf}, and $\Delta C_{p,unf}$. A major aim of this work was to determine the enthalpic and entropic contributions of glycerol to ΔG_{unf}. We first discuss the energetic consequences of glycerol on the cavity mutations (Figure 8, lower panel). In the presence of glycerol, the mutants were enthalpically destabilized in the entire temperature range between 5 and 100 °C, quite different from the situation in water, where $\Delta\Delta H_{unf}$ passes through zero around room temperature. The enthalpy term dominated the destabilization starting from much lower temperature in glycerol (18 °C), compared to plain buffer, where $|\Delta\Delta H_{unf}|$ becomes larger than $|T\Delta\Delta S_{unf}|$ at 50 °C. The reason for the glycerol effect on the transition from entropic to enthalpic destabilization of the cavity mutants is the lower heat capacity change accompanying unfolding in a glycerol/water mixture. A decrease of ΔC_p^{unf} for protein unfolding in water/cosolvent systems has been observed in most other studies, although there are exceptions (*11*, *17*, *41*−*45*). We may try to explain the lower ΔC_p^{unf} in the presence of glycerol by the following reasoning. A positive ΔC_p^{unf} is thought to be a consequence of hydration of nonpolar molecular surface that is not accessible to the solvent in the compact folded state. Polar hydration decreases the unfolding heat capacity, but the total effect is dominated by the large positive heat capacity of nonpolar hydration (*35*, *46*). Since glycerol does not appreciably alter the architecture and solvent accessibility of the folded state, a lower unfolding ΔC_p in water/cosolvent mixtures would indicate that either the water structure around the newly exposed groups in the unfolded peptide is perturbed or the unfolded peptide is, on average, more compact in the mixed solvent than in plain water. We prefer the explanation assuming a more compact unfolded state in glycerol. Two experimental observations support this conjecture. First, the posttransitional portion of the CD melting curves recorded displayed a steeper temperature dependence in glycerol solution than in water. This is an indication of some difference in the nature of the state realized immediately after completion of the main conformational transition in the presence of glycerol. Glycerol induces helix formation in model L-[Lys]$_n$ and L-[Ala]$_n$ peptides and in melittin (*47*). A highly ordered and compact structure of lysozyme in pure glycerol has been reported (*18*). Second, ΔC_p^{unf} of A_2 was decreased by 0.4 kJ K^{-1} mol^{-1} in glycerol while ΔC_p^{unf} of the mutants was decreased by 0.7−0.8 kJ K^{-1} mol^{-1}. If the glycerol effect on ΔC_p^{unf} were to originate solely from hydration of newly exposed molecular surface in the fully solvent-accessible unfolded peptide, one would have predicted the opposite trend since the mutants exposed less nonpolar surface upon unfolding. Reduction of the surface-to-volume ratio implicitly follows from the tendency to decrease the chemical potential, which is raised on transfer of a polypeptide chain from water to a water/glycerol solvent. It has been argued that the unfavorable free energy of transfer of the peptide backbone from water to water/osmolyte solvents (solvophobic effect) substantially raises the chemical potential of the denatured state and leads, as a collateral effect, to a contraction of the denatured ensemble, thus enhancing intermolecular contacts and promoting folding (*48*, *49*). On the other hand, compaction of the unfolded state necessarily restricts its conformational freedom, thus reducing the conformational part of the total unfolding entropy. In contrast, up to about 50 °C, the total unfolding entropy of all three peptides was clearly higher in 30% glycerol than in water. Therefore, we are forced to consider possible effects of the cosolvent on both the native and unfolded state to explain the observed perturbation of energetic unfolding parameters.

What is the origin of increased enthalpy and entropy of unfolding in glycerol (Figure 9)? Using published transfer data (*50*), we calculate a mean enthalpy of transfer of hydrophobic side chains from water to glycerol of 4 ± 2 J mol^{-1} Å^{-2} at 25 °C. If this number represents the typical hydrophobic contribution of apolar surface to the transfer enthalpy in general, the maximal increase of the unfolding enthalpy caused by differences in the solvent structure should be 5−10 kJ mol^{-1} for our leucine zippers. In fact, this is an upper estimate since the calculation assumes that newly exposed apolar surface is completely solvated and neglects the contribution of polar solvation which is of opposite sign (*50*). The experimentally observed increase of the unfolding enthalpy ($\Delta\Delta H_{unf}$) at 25 °C was 3−5 times larger. Obviously, there must be other sources of enthalpic stabilization induced by glycerol. We propose that addition of glycerol enhances

the favorable enthalpic interactions in the folded state. Glycerol decreases the specific volume and the adiabatic compressibility of proteins, probably by causing a collapse of voids in the protein core (*51*). Experimental evidence has been found for local (and possibly global) increase in rigidity, as well as for strong decrease in the conformational heterogeneity of proteins in glycerol/water solvents (*52*, *53*). For example, the thermal backbone fluctuations away from the native state of the *E. coli* galactose/glucose binding protein are greatly reduced by glycerol (*54*). All these effects may intensify the packing interactions in the compact folded state, increasing the enthalpic component to the stability of that state in glycerol. Clearly, the amount of favorable enthalpy accumulated from improved packing interaction should depend on details of the molecular structure. We note that the gain in enthalpy upon transfer from water to 30% glycerol was slightly larger for A_2 than for the mutants. This we may explain by less perfect packing in the cavity mutants. At higher temperatures, the thermal fluctuations of the folded state are enhanced leading to a gradual decrease in the magnitude of enthalpic stabilization. Clearly, a suboptimally packed coiled coil is subjected to larger thermal fluctuations and the packing-related component of the unfolding enthalpy drops more rapidly when temperature increases, as it can be inferred from Figure 9.

A similar argument can explain also the destabilizing entropy effect of glycerol. Water-to-glycerol transfer entropies of some nonpolar amino acids account for only 25% of the observed entropy increase at 25 °C, again as an upper limit (*50*). A better packed, more rigid and less fluctuating folded state is entropically disfavored, the more so in the case of a noncovalently associated dimer, for which vibrational entropy contributions to stability might be considerable (*55*). However, hydration energetics dominates over conformational effects in protein folding. Given the incomplete understanding of the structure of mixed solvents and the ambiguity in the definition of the unfolded state with respect to the extent of solvation and conformational freedom, the assignment of increased total unfolding entropy solely to the restricted conformational flexibility of the folded state is certainly a oversimplification.

Concluding our discussion of the glycerol effect, we would like to remark that the change in protein stability induced by cosolvents is often categorically labeled as enthalpic or entropic. This can be confusing. The enthalpy and entropy of protein unfolding are strongly dependent on the temperature and so are their relative contributions to the changes in unfolding free energy observed in mixed solvents. Depending on the temperature, the enthalpic and entropic terms change not only in magnitude but can also change sign in the experimentally accessible temperature range. Further thermodynamic data, including more reliable estimates of the unfolding heat capacity changes are needed to improve the current understanding about why and how proteins fold in mixed solvents.

ACKNOWLEDGMENT

We thank Hans Rudolf Bosshard for helpful discussions and critical reading of the manuscript. The assistance of Koba Adeishvilli in purification of some peptide samples is acknowledged.

SUPPORTING INFORMATION AVAILABLE

T_m and ΔH_{unf} measured by CD and DSC in plain buffer or in the presence of 30% (w/w) glycerol at different pH values and for different concentrations of A_2 (Table 1), of $(A12)_2$ (Table 2), and of $(A19)_2$ (Table 3). This material is available free of charge via the Internet at http://pubs.acs.org.

REFERENCES

1. Yancey, P. H., Clark, M. E., Hand, S. C., Bowlus, R. D., and Somero, D. N. (1982) *Science 217*, 1214−1222.
2. Somero, G. N., and Clark, M. E. (1985) in *Transport Processes, Iono- and Osmoregulation* (Gilles, R., and Gilles-Baillien, M., Eds.) pp 412−423, Springer-Verlag, New York.
3. Somero, G. N. (1986) *Am. J. Physiol. 251*, R197−R213.
4. Yancey, P. H. (1985) in *Transport Processes, Iono- and Osmoregulation* (Gilles, R., and Gilles-Baillien, M., Eds.) pp 424−436, Springer-Verlag, New York.
5. Kirkwood, J. G., and Goldberg, R. J. (1950) *J. Chem. Phys. 18*, 56−57.
6. Kuntz, I. D., and Kauzmann, W. (1974) *Adv. Protein Chem. 28*, 239−345.
7. Timasheff, S. N. (1993) *Annu. Rev. Biophys. Biomol. Struct. 22*, 65−97.
8. Timasheff, S. N. (1995) in *Protein−Solvent Interactions* (Gregory, R. B., Ed.) pp 445−482, Marcel Dekker Inc.
9. Gekko, K., and Morikawa, T. (1981) *J. Biochem. (Tokyo) 90*, 39−50.
10. Gekko, K., and Timasheff, S. N. (1981) *Biochemistry 20*, 4667−4676.
11. Gekko, K., and Timasheff, S. N. (1981) *Biochemistry 20*, 4677−4686.
12. Gekko, K., and Morikawa, T. (1981) *J. Biochem. (Tokyo) 90*, 51−60.
13. Gekko, K. (1982) *J. Biochem. (Tokyo) 91*, 1197−1204.
14. Cioci, F., and Lavecchia, R. (1994) *Biochem. Mol. Biol. Int. 34*, 705−712.
15. Cioci, F., Lavecchia, R., and Marrelli, L. (1994) *Biocatalysis 10*, 137−147.
16. Cioci, F. (1995) *Enzymol. Microb. Technol. 17*, 592−600.
17. Hammou, H. O., del Pino, I. M. P., and Sanchez-Ruiz, J. M. (1998) *N. J. Chem. 22*, 1453−1461.
18. Knubovets, T., Osterhout, J. J., Connolly, P. J., and Klibanov, A. M. (1999) *Proc. Natl. Acad. Sci. U.S.A. 96*, 1262−1267.
19. Hodges, R. S., Semchuk, P. D., Taneja, A. K., Kay, C. M., Parker, J. M. R., and Mant, C. T. (1988) *Pept. Res. 1*, 19−30.
20. Wendt, H., Leder, L., Harma, H., Jelesarov, I., Baici, A., and Bosshard, H. R. (1997) *Biochemistry 36*, 204−213.
21. Brandts, J. F., and Kaplan, L. J. (1973) *Biochemistry 12*, 2011−2024.
22. Marky, L. A., and Breslauer, K. J. (1987) *Biopolymers 26*, 1601−1620.
23. Kuhlman, B., Luisi, D. L., Young, P., and Raleigh, D. P. (1999) *Biochemistry 38*, 4896−4903.
24. Wyman, J. (1964) *Adv. Protein Chem. 19*, 223−244.
25. Plotnikov, V. V., Brandts, J. M., Lin, L. N., and Brandts, J. F. (1997) *Anal. Biochem. 250*, 237−244.
26. Privalov, P. L., and Potekhin, S. A. (1986) *Methods Enzymol. 131*, 4−51.
27. Rosgen, J., Hallerbach, B., and Hinz, H. J. (1998) *Biophys. Chem. 74*, 153−161.
28. Lumb, K. J., and Kim, P. S. (1995) *Biochemistry 34*, 8642−8648.
29. Zeng, X., Herndon, A. M., and Hu, J. C. (1997) *Proc. Natl. Acad. Sci. U.S.A. 94*, 3673−3678.
30. Dürr, E., Jelesarov, I., and Bosshard, H. R. (1999) *Biochemistry 38*, 870−880.
31. Jelesarov, I., Durr, E., Thomas, R. M., and Bosshard, H. R. (1998) *Biochemistry 37*, 7539−7550.
32. Lacroix, E., Viguera, A. R., and Serrano, L. (1998) *J. Mol. Biol. 284*, 173−191.
33. Fersht, A., and Serrano, L. (1993) *Curr. Opin. Struct. Biol. 3*, 75−83.

34. Buckle, A. M., Cramer, P., and Fersht, A. R. (1996) *Biochemistry 35*, 4298−4305.
35. Makhatadze, G. I., and Privalov, P. L. (1995) *Adv. Protein Chem. 47*, 307−425.
36. Taylor, J. W., Greenfield, N. J., Wu, B., and Privalov, P. L. (1999) *J. Mol. Biol. 291*, 965−976.
37. Jelesarov, I., and Bosshard, H. R. (1996) *J. Mol. Biol. 263*, 344−358.
38. Kohn, W. D., Kay, C. M., and Hodges, R. S. (1995) *Protein Sci. 4*, 237−250.
39. Bhattacharyya, R. P., and Sosnick, T. R. (1999) *Biochemistry 38*, 2601−2609.
40. Bull, H. B., and Breese, K. (1968) *Arch. Biochem. Biophys. 128*, 488−496.
41. Jain, S., and Ahluwalia, J. C. (1997) *Thermochim. Acta 302*, 17−24.
42. Kaushik, J. K., and Bhat, R. (1998) *J. Phys. Chem. B 102*, 7058−7066.
43. Kaushik, J. K., and Bhat, R. (1999) *Protein Sci. 8*, 222−233.
44. Liu, Y. F., and Sturtevant, J. M. (1996) *Biochemistry 35*, 3059−3062.
45. Santoro, M. M., Liu, Y., Khan, S. M., Hou, L. X., and Bolen, D. W. (1992) *Biochemistry 31*, 5278−5283.
46. Murphy, K. P., and Freire, E. (1992) *Adv. Protein Chem. 43*, 313−361.
47. Bello, J. (1993) *Biopolymers 33*, 491−495.
48. Liu, Y., and Bolen, W. D. (1995) *Biochemistry 34*, 12884−12891.
49. Qu, Y., and Bolen, D. W. (1998) *Proc. Natl. Acad. Sci. U.S.A. 95*, 9268−9273.
50. Gekko, K. (1981) *J. Biochem. (Tokyo) 90*, 1643−1652.
51. Priev, A., Almagor, A., Yedgar, S., and Gavish, B. (1996) *Biochemistry 35*, 2061−2066.
52. Bizzarri, A. R., and Cannistraro, S. (1993) *Eur. Biophys. J. 22*, 259−267.
53. Schlyer, B. D., Steel, D. G., and Gafni, A. (1996) *Biochem. Biophys. Res. Commun. 223*, 670−674.
54. Butler, S. L., and Falke, J. J. (1996) *Biochemistry 35*, 10595−10600.
55. Tidor, B., and Karplus, M. (1994) *J. Mol. Biol. 238*, 405−414.

BI992948F